Progress In Electromagnetics Research, PIER 104, 49–67, 2010

NUMERICAL INVESTIGATION OF AN ENERGETIC CONSTRAINT FOR INVERSE SCATTERING PROBLEMS

D. Franceschini

Department of Information Engineering and Computer Science
University of Trento
Via Sommarive, 14, 38123 Trento, Italy

Abstract—Microwave inverse scattering approaches have shown their effectiveness in imaging inaccessible regions. Unfortunately, the problem at hand is strongly non-linear and ill-posed and therefore it is often solved by seeking for the global minimum of a proper functional. Nevertheless, it is also necessary to introduce suitable regularizations in order to improve the convergence of the reconstruction process toward a reliable solution. In this context, the paper presents a method that exploits an energetic constraint to define a regularization term of the cost functional. A numerical validation with single and multiple inhomogeneous lossless targets demonstrates that an improvement of the reconstruction accuracy is achievable without introducing significant computational complexity to the inverse scattering problem.

1. INTRODUCTION

Reliable techniques that allow to investigate in a non-invasive fashion inaccessible areas are of great demand in several applications. Among the available technologies, those exploiting the electromagnetic waves at microwaves frequencies are very appealing to fully retrieve the dielectric and conductivity profiles of unknown scatterers. Such properties may reveal defects in manufactures or civil structures [1–3] (non destructive evaluation and testing of materials) or anomalies in biological tissues and thus support, for example, the diagnosis of breast cancers [4–6]. Moreover, further applications of inverse scattering techniques can be found in the framework of the detection and imaging of buried objects (e.g., [7–10]) and the geophysical inspection of oil reservoirs [11]. In suitable conditions, the retrieval of unknown targets

Corresponding author: D. Franceschini (davide.franceschini@disi.unitn.it).

can be carried out using 2D tomographic approaches [12], however the solution of the challenging 3D vectorial problem is necessary in several situations in order to fully characterize the area under investigation [13–15].

Whatever is the application at hand, the information of the target under test is acquired by sampling the scattered field in a proper region external to the domain to be reconstructed and inverting such measurements. Unfortunately, the inversion techniques have to suitable address many drawbacks intrinsically related to the inverse scattering problem [16]. Firstly, the non-linearity of the mathematical model and the ill-posedness have to be carefully considered [16]. Moreover, unavoidable bounds exist on the collection of independent scattered field data even with multi-view/multi-illumination imaging systems [17, 18]. This issue restricts the quantity of successfully retrievable parameters and therefore it affects the obtainable spatial resolution of the reconstructions of the scatterers under test.

To employ efficient countermeasures for these drawbacks, the inverse scattering problem is usually recast into a minimization of a suitable cost function that measures the discrepancy between the available electromagnetic field data and those estimated through a mathematical model for a trial configuration of the unknowns. When the electromagnetic properties of the target to be imaged are a priori known, the retrieval of the position and the shape can be sufficient. For example, the Level Set method [19, 20] represents an homogeneous object as the zero level of a continuous function and the Linear Sampling technique [21] exploits a suitable indicator function to qualitatively visualize the scatterer support. Moreover, a parametric approach has been recently studied [22] to retrieve the contour of perfectly conducting cylinders. On the contrary, when the complete characterization of the region of investigation is needed, pixel based approaches are often pursued. According to such methods, the area to be reconstructed is partitioned exploiting a suitable discretization grid and the values of the dielectric permittivity and electric conductivity in each cell are usually optimized using deterministic approaches (e.g., gradient search based methods [23, 24]) or stochastic methods [25]. The latters have been widely studied in the microwave imaging context both considering single agent algorithms [26] or multiple agent strategies inspired by the evolutionary biology [27, 28] or by the intelligence of the swarms of insects [29–32].

In order to avoid that such algorithms carry out a blind exploration of the solutions space, a proper cost function is usually exploited to drive the optimization algorithms through the search among the candidate solutions of the inverse scattering problem.

Therefore, the cost function plays a fundamental role in connecting an algorithmic procedure with the physic of the scattering phenomena. Toward this aim, the most adopted approach is based on a cost function composed by two terms. The first one exploits the relationship between the problem unknowns (i.e., the characteristics of the object and the internal field) and the field scattered by the structure under test in a suitable observation region. Besides such a term, the knowledge of the probing field allows one to define a further constraint that takes into consideration the scattering phenomena inside the area to be reconstructed. This introduces a regularization term that favors the convergence of the optimization process toward the true solution.

The above-mentioned constraints obtained from the scattering equations are not the only possible choices and other regularization terms have been studied and successfully applied [33, 34]. In this work, a new regularization term that exploits the principle of the conservation of energy is proposed and analyzed. Starting from such a principle, a constraint between the material properties and the electric field in the investigation region is defined in order to favor the search of the solution that satisfies the Poynting's relationship. The proposed approach does not require any additional a priori knowledge regarding the properties of the scatterers under test or the configuration of the scenario to be imaged. The outline of the paper is as follows. Subsect. 2.1 briefly resumes the formulation of the 2D tomographic scattering problem and in Subsect. 2.2 the proposed regularization term is defined. The 2D scenario has been chosen for this preliminary testing because of its simplicity and its reduced computational complexity with respect to the 3D problem. As far as the numerical validation is concerned, Sect. 3 reports a selected set of representative results to analyze the effectiveness of the introduced regularization term based on energetic constraints. Finally, some conclusions are drawn in Sect. 4.

2. MATHEMATICAL FORMULATION

In this section, the mathematical formulation of the proposed approach is presented. The description of the inverse scattering problem is carried out in Subsect. 2.1, while the details about the regularization term based on the energetic constraint are reported in Subsect. 2.2.

2.1. Problem Statement

Let us consider an unknown scatterer that can be treated as a two-dimensional object (Fig. 1) because its cross section is invariant along

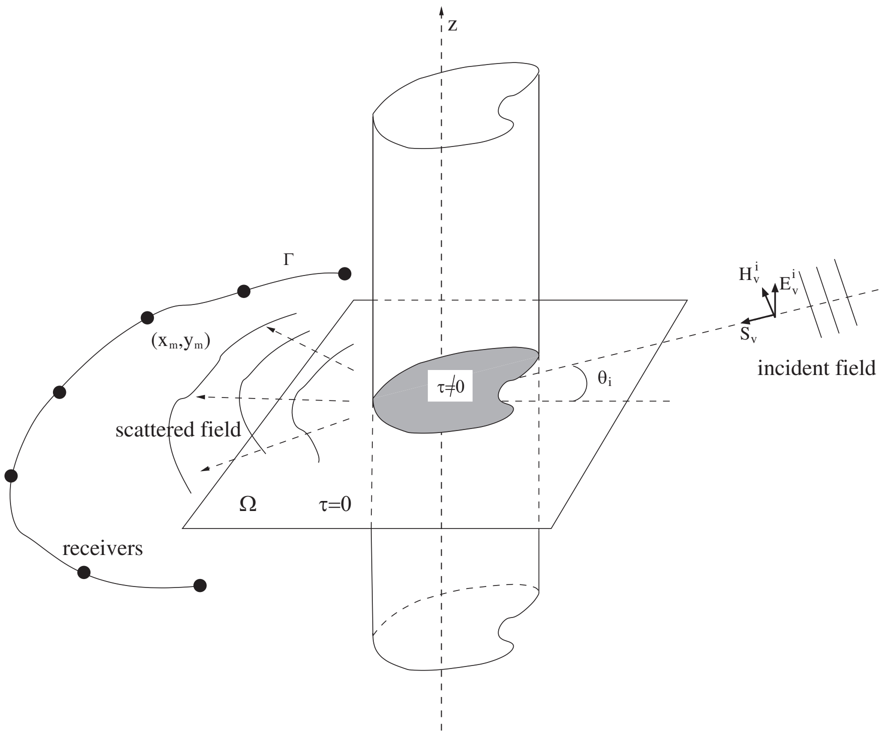

Figure 1. Sketch of the geometry of the tomographic microwave imaging scenario.

the z-axis. Such an object is embedded in a square investigation area, Ω, successively illuminated by a set of known monochromatic TM waves impinging from V different directions, $\mathbf{E}_v^i(x,y) = E_v^i(x,y)\hat{\mathbf{z}}$ ($v = 1,\ldots,V$) being the incident electric field. The characteristics of the unknown target are described by the contrast function $\tau(x,y)$ defined as follows

$$\tau\left(x,y\right) = \varepsilon_r\left(x,y\right) - 1 - j\frac{\sigma\left(x,y\right)}{\omega\varepsilon_o} \tag{1}$$

where ω indicates the fixed angular frequency, ε_o the dielectric permittivity of the vacuum, $\varepsilon_r(x,y)$ and $\sigma(x,y)$ the relative permittivity and the electrical conductivity, respectively. Our aim is to retrieve the distribution of the contrast function (1) relying on the $m(v) = 1,\ldots,M(v)$; $v = 1,\ldots,V$ samples of the scattered field $\mathbf{E}_v^s(x_{m(v)},y_{m(v)}) = E_v^s(x_{m(v)},y_{m(v)})\hat{\mathbf{z}}$ collected in the observation domain Γ surrounding the inaccessible investigation area Ω. Such samples can be obtained from the difference between the field measurements performed in presence and in absence of the scatterer. Moreover, $E_v^s(x_{m(v)}, y_{m(v)})$ can be related to the characteristics of the scenario under test trough the following integral equation ("Data Equation") [16]

$$E_v^s(x_{m(v)}, y_{m(v)}) = k_0^2 \int_\Omega G_{2d}\left(x_{m(v)}, y_{m(v)} | x', y'\right) \tau\left(x', y'\right) E_v^t\left(x', y'\right) dx' dy',$$
$$m_{(v)} = 1, \ldots, M_{(v)} \quad v = 1, \ldots, V \quad (2)$$

where $(x', y') \in \Omega$, $(x_{m(v)}, y_{m(v)}) \in \Gamma$, k_0 is the free space wavenumber and G_{2d} denotes the Green's function of the background medium [35]. $E_v^t(x, y)$ is the internal field, which is also an unknown quantity to be determined by solving the inverse problem. Moreover, as far as the scattering phenomena inside the investigation domain are concerned, they are modeled by means of the "State Equation"

$$E_v^i(x, y) = E_v^t(x, y) - k_0^2 \int_\Omega G_{2d}\left(x, y | x', y'\right) \tau\left(x', y'\right) E_v^t\left(x', y'\right) dx' dy' \quad (3)$$

where $(x,\, y) \in \Omega$.

Because of the ill-conditioning and the intrinsic non-linearity of the inverse scattering problem, Eqs. (2) and (3) are usually solved iteratively determining a sequence of trial solutions for the contrast function and the internal field in order to minimize a suitable cost functional based on the discrepancy between measured $[\tilde{E}_v^s(x_{m(v)}, y_{m(v)}) \in \Gamma]$ or known $[\tilde{E}_v^i(x, y) \in \Omega]$ data and those predicted according to the obtained trial solution. The arising cost function is defined as follows

$$\Phi\left(\tau, E_v^t\right) = \alpha_D \Phi_D\left(\tau, E_v^t\right) + \alpha_S \Phi_S\left(\tau, E_v^t\right) \quad (4)$$

in which the "Data Term" is defined as

$$\Phi_D\left(\tau, E_v^t\right) = \frac{\sum_{v=1}^V \left\| \tilde{E}_v^s\left(x_{m(v)}, y_{m(v)}\right) - E_v^s\left(x_{m(v)}, y_{m(v)}\right) \right\|_\Gamma^2}{\sum_{v=1}^V \left\| \tilde{E}_v^s\left(x_{m(v)}, y_{m(v)}\right) \right\|_\Gamma^2} \quad (5)$$

while the "State Term" is defined as

$$\Phi_S\left(\tau, E_v^t\right) = \frac{\sum_{v=1}^V \left\| \tilde{E}_v^i(x, y) - E_v^i(x, y) \right\|_\Omega^2}{\sum_{v=1}^V \left\| \tilde{E}_v^i(x, y) \right\|_\Omega^2} \quad (6)$$

where $\| \cdot \|_{\Gamma,\Omega}^2$ denotes the L^2-norm on Γ or Ω. Moreover, α_D and α_S are two weighting factors for the data and the state terms, respectively.

The goal is to find the global minimum of the functional (4), which is assumed as the true solution of the inverse scattering problem. Toward this aim, a variety of algorithms based on deterministic or stochastic search approaches can be applied.

2.2. The Energetic Constraint

As described in Subsect. 2.1, the inverse scattering problem is solved by finding the unknowns configuration that minimizes the cost function (4). Such a functional is usually defined considering the "Data Term" [Eq. (5)] and the "State Term" [Eq. (6)] in order to take into account for the scattering phenomena in the observation domain and in the investigation domain, respectively. However, non negligible advantages can be obtained defining further regularization terms, which can exploit constraints available from the physics of the problem or from the a priori information on the scenario under test. For example, in [33] a penalty term has been introduced to consider the knowledge about the homogeneity of the scatterer and thus force the object function to have values equal to zero (background regions) or to a specified contrast. Another study is reported in [34], where a similar approach but based on a multiplicative regularization factor has been proposed.

In this context, a regularization term based on the principle of the conservation of energy is proposed and described in the following. Such an approach does not need a priori information on the scenario under test and it can be exploited to define a further relationship between the electric field internal to the investigation area and the characteristics of the probed medium. Toward this aim, a suitable regularization term needs to be defined. Let us consider the complex Poynting's vector $S_v(x, y)\hat{\mathbf{s}}$ in the frequency domain [36]

$$S_v(x, y)\hat{\mathbf{s}} = \frac{1}{2}\mathbf{E}_v^t(x, y) \times \mathbf{H}_v^{t*}(x, y) \tag{7}$$

where $\hat{\mathbf{s}}$ is a unit vector indicating the direction of $S_v(x, y)$ and $\mathbf{H}_v^t(x, y) = H_{x,v}^t(x, y)\hat{\mathbf{x}} + H_{y,v}^t(x, y)\hat{\mathbf{y}}$ the internal magnetic field, computed from $\mathbf{E}_v^t(x, y)$ through spatial derivatives that can be numerically evaluated using a finite difference method [38].

If we assume an isotropic lossless medium and a source free region, $\mathrm{Re}\{S_v(x, y)\}$ and $\mathrm{Im}\{S_v(x, y)\}$ satisfy the following differential relationships [36]

$$\nabla \cdot \mathrm{Re}\left\{S_v(x, y)\right\}\hat{\mathbf{s}} = 0 \tag{8}$$

$$\begin{aligned}\nabla \cdot \mathrm{Im}\left\{S_v(x, y)\right\}\hat{\mathbf{s}} + \frac{\omega}{2}\big\{&\mu_0\mathbf{H}_v^t(x, y)\cdot\mathbf{H}_v^{t*}(x, y) + \\ &-\varepsilon_o\left[\mathrm{Re}\left\{\tau\left(x, y\right)\right\} + 1\right]\mathbf{E}_v^t(x, y)\cdot\mathbf{E}_v^{t*}(x, y)\big\} = 0\end{aligned} \tag{9}$$

where the symbol * denotes the complex conjugate.

Equation (8) represents a constraint on $\mathrm{Re}\{S_v(x, y)\}$ (i.e., on the total field $E_v^t(x, y)$) and Eq. (9) a bond between the unknowns of the internal field $E_v^t(x,y)$, $v = 1,\ldots,V$, and the real part of the contrast function $\mathrm{Re}\{\tau(x,y)\}$ (for the specific case of lossless scatterers).

In order to investigate whether the relationships (8) and (9) improve the effectiveness of the reconstruction process, a proper regularization term has been defined. To numerically deal with the optimization of the unknown parameters, the integral Eqs. (2) and (3) are discretized considering the method of moments (MoM) [37] and therefore $\tau(x,y)$ and $E_v^t(x,y)$ in Ω are represented through a linear combination of piecewise constant functions (Λ_n, $n = 1,\ldots,N$) as follows

$$\tau\left(x,y\right) \simeq \sum_{n=1}^{N} \tau\left(x_n,y_n\right)\Lambda_n\left(x,y\right), \tag{10}$$

$$E_v^t(x,y) \simeq \sum_{n=1}^{N} E_v^t(x_n,y_n)\Lambda_n\left(x,y\right) \tag{11}$$

N being the number of subdomains in which the investigation domain Ω is partitioned. Each subdomain V_n, $n = 1,\ldots,N$, is centered in (x_n,y_n) and $\Lambda_n(x,y) = 1$ if $(x,y) \in V_n$, while $\Lambda_n(x,y) = 0$ otherwise.

Equations (8) and (9) hold in every cell $V_n \in \Omega$ of the discretization grid, therefore the following term can be defined to take into account for the conservation of energy during the solution of the inverse scattering problem

$$\begin{aligned}\Phi_E \;=\; & \frac{1}{NV}\sum_{v=1}^{V}\sum_{n=1}^{N}\left|\nabla\cdot\mathrm{Re}\left[S_v\left(x_n,y_n\right)\hat{\mathbf{s}}\right]+j\nabla\cdot\mathrm{Im}\left[S_v\left(x_n,y_n\right)\hat{\mathbf{s}}\right]\right.\\ & +j\frac{\omega}{2}\left\{\mu_0\mathbf{H}_v^t(x,y)\cdot\mathbf{H}_v^{t*}(x,y)-\varepsilon_o\left\{\mathrm{Re}\left[\tau\left(x_n,y_n\right)\right]+1\right\}\right.\\ & \left.\left.\mathbf{E}_v^t(x,y)\cdot\mathbf{E}_v^{t*}(x,y)\right\}\right|^2\end{aligned} \tag{12}$$

where the divergence operator as well as $S_v(x_n,y_n)\hat{\mathbf{s}}$ and $\mathbf{H}_v^t$ can be numerically computed using a finite difference method [38].

The term (12) can be added to the "Data" and "State" terms of Eq. (4) in order to define a new cost function as follows

$$\Phi\left(\tau,E_v^t\right) = \alpha_D\Phi_D\left(\tau,E_v^t\right)+\alpha_S\Phi_S\left(\tau,E_v^t\right)+\alpha_E\Phi_E\left(\tau,E_v^t\right) \tag{13}$$

in which α_E indicated the weighting factor for the energetic term of the functional. In order to minimize the cost function (13), a conjugate gradient search technique has been employed for a preliminary investigation of the effectiveness of the term Φ_E. As a matter of fact, a deterministic strategy allows us to analyze the benefit of the proposed approach without the need of additional unavoidable processing connected with the stochastic nature of evolutionary algorithms (e.g., [28, 30]).

3. NUMERICAL VALIDATION

The effectiveness of the energetic constraint in the context of the inverse scattering problems is assessed in this section considering a set of selected representative experiments regarding the reconstruction of two-dimensional lossless profiles. The test case presented in Subsect. 3.1 is concerned with a layered contrast. Some reconstruction results are discussed and a numerical analysis of some error figures is reported in order to investigate the robustness of the proposed approach. Moreover, Subsect. 3.2 presents the results regarding a more complex multiple scatterers configuration to provide further confirmations of the improved accuracy achievable employing the proposed constraint.

3.1. Layered Scatterer

The reference geometry of the first test case shown in Fig. 2 is a layered cylinder located at $x_c^{ref} = y_c^{ref} = 0.0\lambda$ (λ being the free space wavelength) in a square investigation domain $L_\Omega = 1.0\lambda$-sided. The object function of the outer square layer ($L_{out} = 0.7\lambda$-sided) is $\tau_1 = 1.0$ while the inner layer ($L_{in} = 0.3\lambda$-sided) is characterized by $\tau_2 = 2.0$ and is centered at $(x_{in}, y_{in}) = (0.1\lambda, 0.05\lambda)$. The investigation domain has been illuminated by plane waves impinging from $V = 8$ equally-spaced directions ($\theta_i = (v-1)\frac{\pi}{4}$, $v = 1, \ldots, V$). For each incidence,

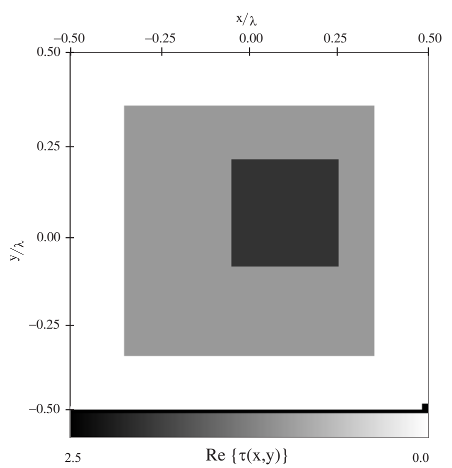

Figure 2. *Single layered profile.* Reference distribution of the object function.

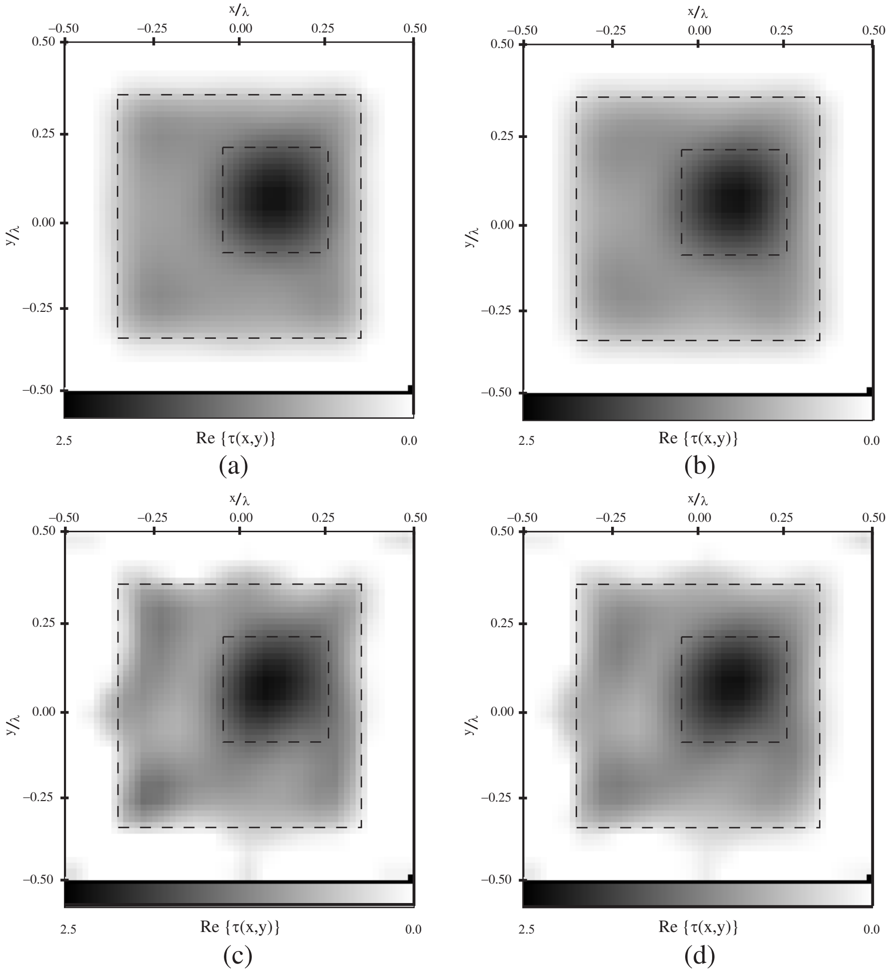

Figure 3. *Single layered profile.* Reconstructed contrast with (a) (c) $\alpha_E = 0$ and (b) (d) $\alpha_E = 1$ using (a) (b) noise free data and (c) (d) noisy data ($SNR = 20\,\text{dB}$).

the scattered field is measured at $M(v) = 35$ positions and the synthetically computed data have been blurred adding a Gaussian noise. The reconstruction procedure has been carried out discretizing Ω with $N = 400$ subdomains ad using equally weighted term in the cost function (13): $\alpha_D = \alpha_S = \alpha_E = 1.0$.

The first set of results of the retrieved profiles is reported in Fig. 3. The contrast functions of Figs. 3(a), (c) show the reconstruction accuracy achieved through a standard conjugate gradient-based algorithm† that minimizes the cost functional composed only by the "Data" and "State" terms. Fig. 3(a) refers to the noiseless case, while Fig. 3(c) to an experiment in which a Gaussian noise of signal-to-noise ratio (SNR) of 20 dB has been added to the scattered field measures. As it can be observed, the results are satisfactory and the layered profile is clearly distinguishable (the dashed lines indicate the boundaries of the two layers). To have some quantitative parameters to compare the retrieved targets, the following reconstruction error figures have been defined

$$\zeta_{(j)} = \frac{1}{N_{(j)}} \sum_{n=1}^{N_{(j)}} \left\{ \frac{\tau(x_n, y_n) - \tau^{ref}(x_n, y_n)}{\tau^{ref}(x_n, y_n)} \right\} \times 100 \tag{14}$$

where $N_{(j)}$ can range over the whole investigation domain ($j \Rightarrow tot$), or over the area where the actual scatterer is located ($j \Rightarrow int$), or over the background belonging to the investigation domain ($j \Rightarrow ext$). τ^{ref} indicates the reference value of the actual object function of the pixel centered in (x_n, y_n). According to such definitions, the values of the overall reconstruction error (ζ_{tot}) for the profiles of Figs. 3(a), (c) are lower than 8% (see Tab. 1).

Table 1. *Single layered profile.* Values of the error figures of the reconstructed contrast for different SNRs ($\alpha_E = 0.0$).

SNR [dB]	ζ_{tot}	ζ_{int}	ζ_{ext}
Noiseless	7.46	8.25	6.73
20	7.18	9.38	5.06
10	26.31	45.09	8.28
5	33.36	54.19	13.35

Table 2. *Single layered profile.* Values of the error figures of the reconstructed contrast for different SNRs ($\alpha_E = 1.0$).

SNR [dB]	ζ_{tot}	ζ_{int}	ζ_{ext}
Noiseless	8.17	8.66	7.70
20	7.91	9.23	6.64
10	12.41	16.31	8.67
5	21.70	27.60	16.04

The same experiments have been carried out also exploiting the energetic term as described in the cost functional (13). From Figs. 3(b), (d) and from the values of ζ_{tot} reported in Tab. 2 one can notice that the exploitation of the energy conservation principle has not provided any substantial improvement to the reconstruction accuracy.

Successively, further experiments have been performed with the same test case but decreasing the SNR to 10 dB [Figs. 4(a), (b)] and 5 dB [Figs. 4(c), (d)]. The results of such numerical simulations

† The background characteristics and the incident field configuration have been considered as initial guess for the contrast function and the internal field, respectively.

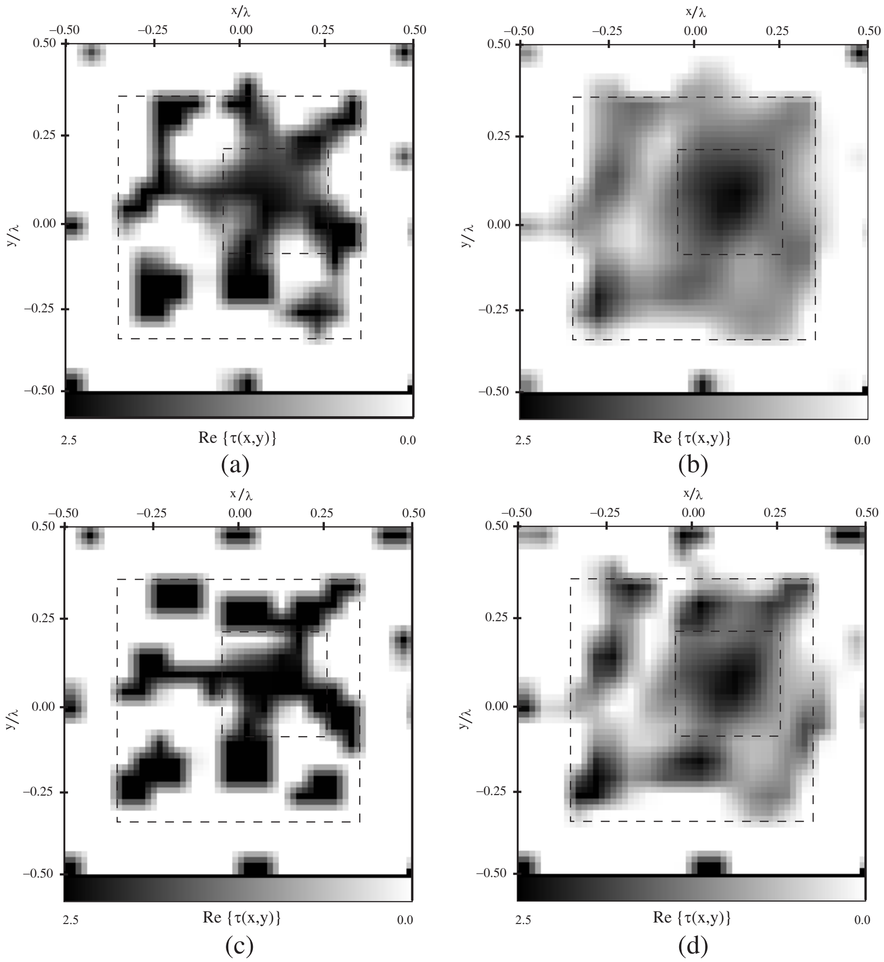

Figure 4. *Single layered profile.* Reconstructed contrast with (a) (c) $\alpha_E = 0$ and (b) (d) $\alpha_E = 1$ — Noisy data: (a) (b) $SNR = 10\,\mathrm{dB}$ and (c) (d) $SNR = 5\,\mathrm{dB}$.

show the effectiveness of the energetic constraint, which contributes to considerably improve the accuracy of the retrieved scatterer. If we compare Fig. 4(a) with Fig. 4(b), the latter provides a clear estimate of the shape of the square profile, as well as of the inhomogeneity of the object function. This does not hold when Φ_E is not exploited [Fig. 4(a)]. Such qualitative observations are confirmed by the reconstruction errors reported in Tab. 1 and Tab. 2. It is pointed out that ζ_{tot} decreases from 26.31% to 12.41% when the optimization process is forced to search for a solution that satisfies the energetic constraint and $\zeta_{int}^{\alpha_E=0} \simeq 45\%$ versus $\zeta_{int}^{\alpha_E=1} \simeq 16\%$. Similar comments hold for the experiments carried out with $SNR = 5\,\text{dB}$ [compare Fig. 4(c) with Fig. 4(d) and the error figures in Tab. 1 and Tab. 2].

In the following, let us further analyze if the achieved performances can be related to the effectiveness of the energetic constraint. Toward this aim, Fig. 5 presents color level maps in which each pixel pictorially shows the values of $\Psi_E^{v=1}(x_n, y_n)$, $n = 1, \ldots, N$, being

$$\begin{aligned}\Psi_E^{v=1}(x_n, y_n) = \Big| & \nabla \cdot \mathrm{Re}\left[S_1\left(x_n, y_n\right)\hat{\mathbf{s}}\right] + j\nabla \cdot \mathrm{Im}\left[S_1\left(x_n, y_n\right)\hat{\mathbf{s}}\right] \\ & + j\frac{\omega}{2}\left\{\mu_0 \mathbf{H}_1^t(x, y) \cdot \mathbf{H}_1^{t*}(x, y) - \varepsilon_o \left\{\mathrm{Re}\left[\tau\left(x_n, y_n\right)\right] + 1\right\}\right. \\ & \left.\mathbf{E}_1^t(x, y) \cdot \mathbf{E}_1^{t*}(x, y)\right\}\Big| \end{aligned} \tag{15}$$

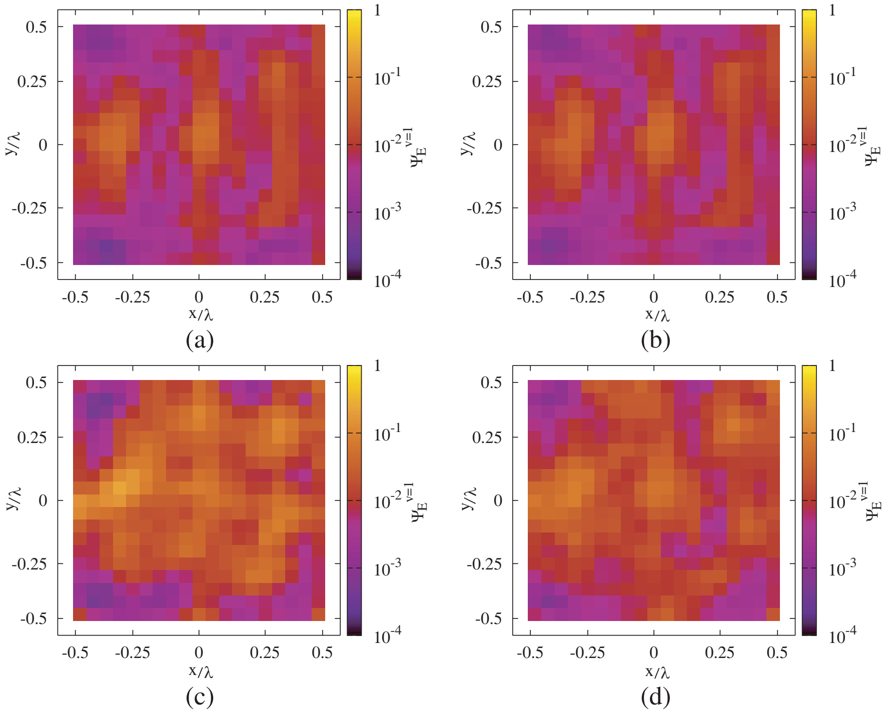

Figure 5. *Single layered profile.* Plots of the discrepancy $\Psi_E^{v=1}$ in the investigation area. Distributions concerning the reconstructed contrast with (a) (c) $\alpha_E = 0$ and (b) (d) $\alpha_E = 1$ [test cases concerned with the simulation at (a) (b) $SNR = 20\,\text{dB}$ and (c) (d) $SNR = 10\,\text{dB}$].

The plots of $\Psi_E^{v=1}$ concerning the contrast function of Figs. 3(c), (d) and Figs. 4(a), (b) are reported in Figs. 5(a), (b) and Figs. 5(c), (d), respectively. Fig. 5(a) and Fig. 5(b) are clearly similar: The mean value of $\Delta\Psi_{E,\,20\,\mathrm{dB}}^{v=1} = |\Psi_{E,\,20\,\mathrm{dB}}^{v=1,\alpha_E=0} - \Psi_{E,\,20\,\mathrm{dB}}^{v=1,\alpha_E=1}|$ is 7.52×10^{-4}. This is consistent with the resemblance of the retrieved profiles of Fig. 3(c) and Fig. 3(d). Therefore, when the problem data are slightly corrupted by noise ($SNR \geq 20\,\mathrm{dB}$), the optimization process is capable to achieve a convergence solution that satisfies the energetic constraint also without employing the term Φ_E. On the contrary, observing Fig. 5(c) it is noticed that the values of $\Psi_E^{v=1}(x_n, y_n)$ computed considering the convergence solution achieved when $\alpha_E = 0$ are higher than those of Fig. 5(d), obtained exploiting the energetic constraint. The mean value of $\Delta\Psi_{E,\,10\,\mathrm{dB}}^{v=1}$ is 1.37×10^{-2}. Consequently, the retrieved profile of Fig. 4(a) do not satisfy very well the constraint (15) while non negligible advantages [Fig. 4(b)] are obtained with a configuration of the unknown parameters that better fits (15).

Before performing further numerical assessments with different test cases, it is worth analyzing the impact of the choice of α_E, i.e., the optimal weight of the term Φ_E. Toward this aim, several reconstructions of the reference object of Fig. 2 have been performed setting $0.0 \leq \alpha_E \leq 10.0$. The data have been blurred with a Gaussian noise characterized by $SNR = 10\,\mathrm{dB}$ for the whole set of numerical simulations. Fig. 6 resumes the achieved results in term of reconstruction errors. For calibration purposes, let us focus on the behavior of ζ_{tot}. In the range $0.6 \leq \alpha_E \leq 2.5$ the variation of ζ_{tot} is less that 1%, therefore no appreciable differences are noted in the final reconstructions when the value α_E is set within such an interval.

3.2. Multiple Scatterers

In order to further investigate the indications drawn from the numerical experiments of Subsect. 3.1, an additional validation has been performed considering the multiple scatterers scenario of Fig. 7. The first object is a cylinder centered at ($x_c^{(1)} = -0.1\lambda$, $y_c^{(1)} = 0.30\lambda$) with a rectangular cross-section of height $h = 0.2\lambda$ and width $w = 0.6\lambda$. The contrast function of such a target is homogeneous ($\tau^{(1)} = 2.5$). On the contrary, the square scatterer is inhomogeneous ($\tau^{(2)} = 2.0$ and $\tau^{(3)} = 1.0$), 0.4λ sided and centered at ($x_c^{(2)} = 0.15\lambda$, $y_c^{(2)} = -0.15\lambda$). The configuration of the measurement setup as well as the simulations parameters are the same used in the experiments concerned with the single scatterer of Subsect. 3.1. The gray-level representations of the retrieved profiles are reported in Fig. 8 for $SNR = 10\,\mathrm{dB}$

[Figs. 8(a), (b)] and $SNR = 5\,\mathrm{dB}$ [Figs. 8(c), (d)]. Figs. 8(a), (c) have been obtained using the reference approach ($\alpha_E = 0.0$) while in the experiments of Figs. 8(b), (d) $\alpha_E = 1.0$. It is clearly noticed that the accuracy of the reconstructed object function is more satisfactory when the term that takes into account for the conservation of energy is employed [compare Fig. 8(a) vs. Fig. 8(b) and Fig. 8(b) vs. Fig. 8(d)]. This can be numerically confirmed computing the reconstruction errors, whose values are reported in Tab. 3. If the term Φ_E is exploited, the total reconstruction error decreases, being

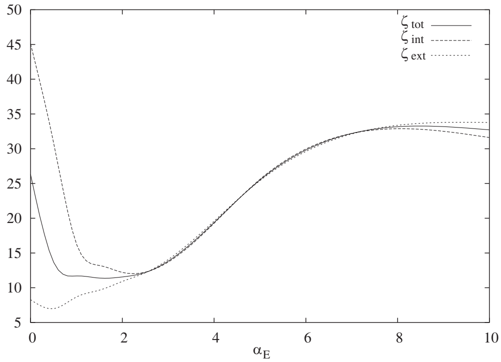

Figure 6. *Single layered profile.* Behavior of the reconstruction error figures for different weights (α_E) of the the energetic term ($SNR = 10\,\mathrm{dB}$).

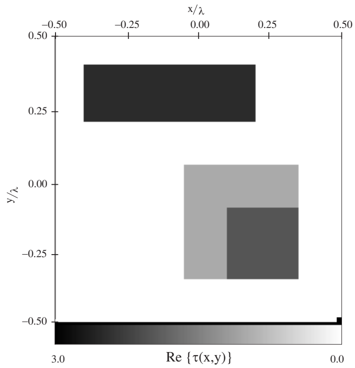

Figure 7. *Multiple scatterers profile.* Reference distribution of the object function.

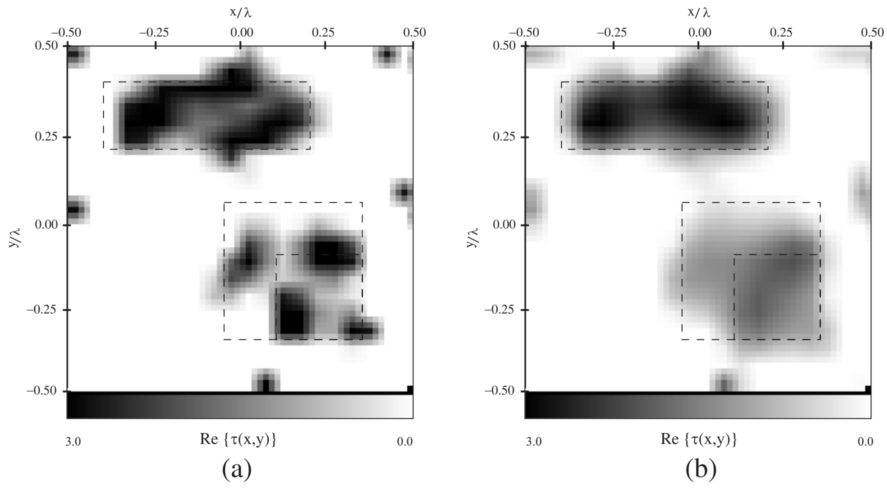

(a) (b)

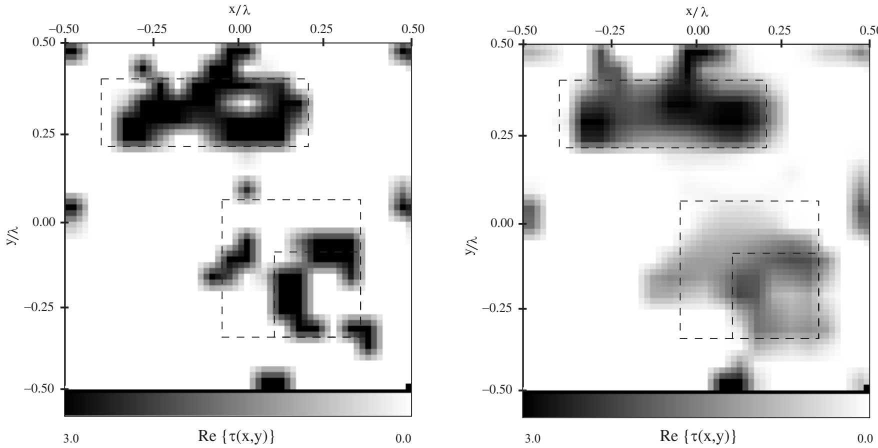

(c) (d)

Figure 8. Multiple scatterers profile. Reconstructed contrast with (a) (c) $\alpha_E = 0$ and (b) (d) $\alpha_E = 1$ — Noisy data: (a) (b) $SNR = 10\,\mathrm{dB}$ and (c) (d) $SNR = 5\,\mathrm{dB}$.

Table 3. *Multiple scatterers profile.* Values of the error figures of the contrast retrieved with and without exploiting the energetic constraint — Noisy data: $SNR = 10\,\mathrm{dB}$ and $SNR = 5\,\mathrm{dB}$.

	ζ_{tot}	ζ_{int}	ζ_{ext}
$\alpha_E = 0.0$; $SNR = 10\,[\mathrm{dB}]$	17.28	32.18	11.49
$\alpha_E = 0.0$; $SNR = 5\,[\mathrm{dB}]$	23.87	42.92	16.46
$\alpha_E = 1.0$; $SNR = 10\,[\mathrm{dB}]$	14.51	17.26	13.44
$\alpha_E = 1.0$; $SNR = 5\,[\mathrm{dB}]$	21.69	22.70	21.30

$\zeta_{tot}^{\alpha=1} = 84\%\zeta_{tot}^{\alpha=0}$ and $\zeta_{tot}^{\alpha=1} = 91\%\zeta_{tot}^{\alpha=0}$ for the reconstructions at $SNR = 10\,\mathrm{dB}$ and $SNR = 5\,\mathrm{dB}$, respectively. Moreover, let us also consider the parameter ζ_{int} in order to estimate the reconstruction accuracy in the regions effectively occupied by the true scatterers. The improvement of the quality of the retrieved targets is very satisfactory, being $\zeta_{int}^{\alpha=1} = 54\%\zeta_{int}^{\alpha=0}$ the internal error at $SNR = 10\,\mathrm{dB}$ and $\zeta_{int}^{\alpha=1} = 53\%\zeta_{int}^{\alpha=0}$ the same parameter at $SNR = 5\,\mathrm{dB}$.

Finally, Fig. 9 depicts the behavior of the reconstruction error ζ_{tot} according to different choices of the weighting parameter α_E. Several experiments have been performed setting the signal-to-noise ratio of the Gaussian noise to 50 dB, 20 dB and 10 dB. As can be observed from

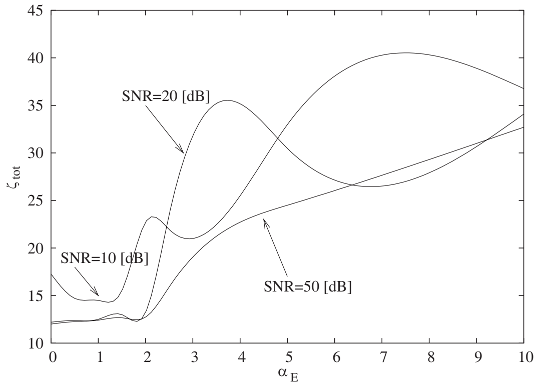

Figure 9. Multiple scatterers profile. Behavior of the reconstruction error ζ_{tot} for different values of α_E ($50\,\mathrm{dB} \geq SNR \geq 5\,\mathrm{dB}$).

Fig. 9, the value of $\alpha_E = 1.0$ lies about in the center of a plateau where the computed reconstruction error reaches the minimum values. No significant variation of ζ_{tot} has been noticed choosing $0.5 \leq \alpha_E \leq 1.3$. Therefore the choice of $\alpha_E = 1$ can be satisfactory.

4. CONCLUSION

In the context of microwave imaging problems, this paper has presented an energetic constraint to improve the effectiveness of inverse scattering methodologies. The numerical experiments concerned with layered and multiple scatterers configurations have shown that, as expected, in ideal noiseless situations or in case of low-noise experiments the standard approach based on the "Data" and "State" equations already provides accurate solutions, whose configurations satisfy the energetic constraint. On the contrary, when the data are significantly corrupted by noise as it may occurs in practical applications, the proposed approach provides satisfactory improvements in the quality of the retrieved contrasts. Further studies are currently being pursued in order to carry out an experimental validation of the proposed approach also considering more complex lossy profiles.

REFERENCES

1. Bolomey, J. C., *Frontiers in Industrial Process Tomography*, Engineering Foundation, New York, 1995.

2. Benedetti, M., M. Donelli, and A. Massa, "Multicrack detection in two-dimensional structures by means of GA-based strategies," *IEEE Trans. Antennas Propagat.*, Vol. 55, 205–215, Jan. 2007.
3. Kharkovsky, S. and R. Zoughi, "Microwave and millimeter wave nondestructive testing and evaluation — Overview and recent advances," *IEEE Instrum. and Meas. Mag.*, Vol. 10, 26–38, Apr. 2007.
4. Meaney, P. M., M. W. Fanning, L. Dun, S. P. Poplack, and K. D. Paulsen, "A clinical prototype for active microwave imaging of the breast," *IEEE Trans. Microwave Theory Tech.*, Vol. 48, 1841–1853, Nov. 2000.
5. O'Halloran, M., R. Conceicao, D. Byrne, M. Glavin, and E. Jones, "FDTD modeling of the breast: A review," *Progress In Electromagnetics Research B*, Vol. 18, 1–24, 2009.
6. Lazaro, A., D. Girbau, and R. Villarino, "Simulated and experimental investigation of microwave imaging using UWB," *Progress In Electromagnetic Research*, PIER 94, 263–280, 2009.
7. Cui, T. J., W. C. Chew, A. A. Aydiner, and S. Chen, "Inverse scattering of two-dimensional dielectric objects buried in a lossy earth using the distorted Born iterative method," *IEEE Trans. Geosci. Remote Sensing*, Vol. 39, 339–346, Feb. 2001.
8. Bermani, E., A. Boni, S. Caorsi, and A. Massa, "An innovative real-time technique for buried object detection," *IEEE Trans. Geosci. Remote Sensing*, Vol. 41, 927–931, 2003.
9. Crocco, L., M. D'Urso, and T. Isernia, "The contrast source-extended Born model for 2D subsurface scattering problems," *Progress In Electromagnetics Research B*, Vol. 17, 343–359, 2009.
10. Catapano, I., L. Crocco, R. Persico, M. Pieraccini, and F. Soldovieri, "Linear and nonlinear microwave tomography approaches for subsurface prospecting: Validation on real data," *IEEE Antennas Wireless Propag. Lett.*, Vol. 5, 49–53, Dec. 2006.
11. Zhang, Z. Q. and Q. H. Liu, "Applications of the BiCGS-FFT method to 3-D induction well logging problems," *IEEE Geosci. Remote Sensing*, Vol. 41, 856–869, May 2003.
12. Caorsi, S., A. Massa, M. Pastorino, and M. Donelli, "Improved microwave imaging procedure for nondestructive evaluations of two-dimensional structures," *IEEE Trans. Antennas Propagat.*, Vol. 52, 1386–1397, 2004.
13. Yu, Y., T. Yu, and L. Carin, "Three-dimensional inverse scattering of a dielectric target embedded in a lossy half-space," *IEEE Trans. Geosci. Remote Sensing*, Vol. 42, 957–973, May 2004.

14. Li, F., Q. H. Liu, and L.-P. Song, "Three dimensional reconstruction of objects buried in layered media using Born and distorted Born iterative methods," *IEEE Trans. Geosci. Remote Sensing*, Vol. 1, 107–111, Apr. 2004.
15. Franceschini, G., A. Abubakar, T. M. Habashy, and A. Massa, "A comparative assessment among iterative linear solvers dealing with electromagnetic integral equations in 3D inhomogeneous anisotropic media," *Journal of Electromagnetic Waves and Applications*, Vol. 21, No. 7, 899–914, 2007.
16. Colton, D. and R. Krees, *Inverse Acoustics and Electromagnetic Scattering Theory*, Springer-Verlag, Berlin, Germany, 1992.
17. Bucci, O. M. and T. Isernia, "Electromagnetic inverse scattering: Retrievable information and measurement strategies," *Radio. Sci.*, Vol. 32, 2123–2138, Dec. 1997.
18. Bucci, O. M., L. Crocco, T. Isernia, and V. Pascazio, "Subsurface inverse scattering problems: Quantifying, qualifying and achieving the available information," *IEEE Trans. Geosci. Remote Sensing*, Vol. 39, 2527–2537, Nov. 2001.
19. Litman, A., "Reconstruction by level sets of N-ary scattering obstacles," *Inv. Probl.*, Vol. 21, S131–S152, Dec. 2005.
20. Dorn, O. and D. Lesselier, "Level set methods for inverse scattering," *Inv. Probl.*, Vol. 22, R67–R131, Aug. 2006.
21. Aramini, R., M. Brignone, and M. Piana, "The linear sampling method without sampling," *Inv. Probl.*, Vol. 22, 2237–2254, Dec. 2006.
22. Rekanos, I. T., "Shape reconstruction of a perfectly conducting scatterer using differential evolution and particle swarm optimization," *IEEE Trans. Geosci. Remote Sensing*, Vol. 46, 1967–1974, Jul. 2008.
23. Kleinman, R. E. and P. M. van den Berg, "A modified gradient method for two-dimensional problems in tomography," *J. Comput. Appl. Math.*, Vol. 42, 17–35, 1992.
24. Van den Berg, P. M. and A. Abubakar, "Contrast source inversion method: State of the art," *Progress In Electromagnetics Research*, PIER 34, 189–218, 2001.
25. Rocca, P., M. Benedetti, M. Donelli, D. Franceschini, and A. Massa, "Evolutionary optimization as applied to inverse scattering problems," *Inv. Probl.*, Vol. 25, No. 12, Article No. 123003, Dec. 2009.
26. Garnero, L., A. Franchois, J.-P. Hugonin, C. Pichot, and N. Joachimowicz, "Microwave imaging-complex permittivity

reconstruction by simulated annealing," *IEEE Trans. Microwave Theory Tech.*, Vol. 39, 1801–1807, Nov. 1991.
27. Caorsi, S., A. Massa. and M. Pastorino, "A computational technique based on a real-coded genetic algorithm for microwave imaging purposes," *IEEE Trans. Geosci. Remote Sensing*, Vol. 38, 1697–1708, Jul. 2000.
28. Caorsi, S., A. Massa, M. Pastorino, and A. Randazzo, "Electromagnetic detection of dielectric scatterers using phaseless synthetic and real data and the memetic algorithm," *IEEE Trans. Geosci. Remote Sensing*, Vol. 41, 2745–2753, 2003.
29. Caorsi, S., M. Donelli, A. Lommi, and A. Massa, "Location and imaging of two-dimensional scatterers by using a particle swarm algorithm," *Journal of Electromagnetic Waves and Applications*, Vol. 18, 481–494, 2004.
30. Donelli, M. and A. Massa, "Computational approach based on a particle swarm optimizer for microwave imaging of two-dimensional dielectric scatterers," *IEEE Trans. Microwave Theory Tech.*, Vol. 53, 1761–1776, May 2005.
31. Donelli, M., G. Franceschini, A. Martini, and A. Massa, "An integrated multiscaling strategy based on a particle swarm algorithm for inverse scattering problems," *IEEE Trans. Geosci. Remote Sensing*, Vol. 44, 298–312, 2006.
32. Huang, T. and A. S. Mohan, "A microparticle swarm optimizer for the reconstruction of microwave images," *IEEE Trans. Antennas Propagat.*, Vol. 55, 568–576, Mar. 2007.
33. Crocco, L. and T. Isernia, "Inverse scattering with real data: Detecting and imaging homogeneous dielectric objects," *Inv. Probl.*, Vol. 17, 1573–1583, Dec. 2001.
34. Abubakar, A., P. M. van den Berg, and S. Y. Semenov, "Two- and three-dimensional algorithms for microwave imaging and inverse scattering," *Journal of Electromagnetic Waves and Applications*, Vol. 17, No. 2, 209–231, Feb. 2003.
35. Jones, D. S., *The Theory of Electromagnetism*, Pergamon Press, Oxford, U.K., 1964.
36. Franceschetti, G., *Elctromagnetics: Theory, Techniques, and Engineering Paradigms*, Plenum Press, New York, London, 1997.
37. Richmond, J. H., "Scattering by a dielectric cylinder of arbitrary cross section shape," *IEEE Trans. Antennas Propagat.*, Vol. 13, 334–341, May 1965.
38. Burden, R. L. and J. D. Faires, *Numerical Analysis*, Brooks-Cole, Pacific Grove, CA, 2001.